

Linear resonance in viscous films on inclined wavy planes

A. Wierschem^{a,b,*}, V. Bontozoglou^c, C. Heining^a, H. Uecker^d, N. Aksel^a

^a Applied Mechanics and Fluid Dynamics, University of Bayreuth, D-95440 Bayreuth, Germany

^b Process Systems Engineering, Technical University of Munich, Weihenstephaner Steig 23, D-85350 Freising, Germany

^c Department of Mechanical and Industrial Engineering, University of Thessaly, Pedion Areos, GR-38334 Volos, Greece

^d Institute of Mathematics, Carl-von-Ossietzky-University, D-26111 Oldenburg, Germany

Received 11 May 2007; received in revised form 6 December 2007

Abstract

We study viscous gravity-driven films flowing over periodically undulated substrates. Linear analysis describes steady flow along small amplitude corrugations for films of arbitrary thickness. Solving the resulting system numerically, we demonstrate resonance (or, possibly, near resonance) and identify different behaviours for thin, intermediate and thick films. Approximating the leading-order velocity profile by the free surface value allows for an analytic solution, which – in the limit of high Reynolds numbers – recovers the different regimes and reveals the relevant physical mechanisms. Our results support the view that the resonance is associated with an interaction of the undulated film with capillary-gravity waves travelling against the mean flow direction. As a consequence, the resonance peak is attained under conditions that render the wave phase velocity equal to zero in the laboratory reference frame, and thus permit direct exchange of energy between the steadily deformed film and the free surface.

© 2008 Elsevier Ltd. All rights reserved.

Keywords: Resonance; Capillary-gravity waves; Free-surface flow; Bottom undulation; Orr–Sommerfeld equation; Linear stability

1. Introduction

The flow of a viscous liquid down a wavy incline is an extension of the paradigmatic gravity-driven film over a flat incline (Chang, 1994) to study the effect of curved substrates on the film flow. It is of great importance, since in many industrial and environmental systems the substrates are usually curved or undulated (Focke and Knibbe, 1986; deSantos et al., 1991; Webb, 1994). For monotonously falling bottom contours, the local steady flow of thin films at low Reynolds numbers corresponds essentially to that over a flat incline at the local inclination angle (Wang, 1984; Shetty and Cerro, 1993; Wierschem et al., 2005). A general formulation of the problem of film flow

along a curved substrate has recently been provided by Roberts and Li (2006). On a flat incline, surface waves or shear waves are generated beyond a critical Reynolds number (Benjamin, 1957; Yih, 1963; Lin, 1967; Floryan et al., 1987). The onset of the surface waves in flow over an undulated substrate deviates continuously with increasing steepness from that for the flat plane (Wierschem et al., 2005; Argyriadi et al., 2006).

Apart from the aforementioned qualitative similarities, film flow over wavy bottoms also shows phenomena that cannot be found in the flow down a flat incline: at moderate steepness, hydraulic jumps are generated at the inflow into the flat region of the undulated bottom (Wierschem and Aksel, 2004a). At high Reynolds numbers, surface waves can be suppressed and are eventually replaced by three-dimensional instabilities (Vlachogiannis and Bontozoglou, 2002; Wierschem and Aksel, 2004b). Besides detachment at the lee side of bottom undulations (Malamataris and Bontozoglou, 1999), eddies form at the flat side of the bottom contour at certain Reynolds numbers (Negny

* Corresponding author. Address: Process Systems Engineering, Technical University of Munich, Weihenstephaner Steig 23, D-85350 Freising, Germany. Tel.: +49 8161 71 3727; fax: +49 8161 71 4510.

E-mail address: wiersche@wzw.tum.de (A. Wierschem).

et al., 2001) or in the valleys of steeply undulated bottoms even in creeping flows (Zhao and Cerro, 1992; Kang and Chen, 1995; Scholle et al., 2004).

Recently, Luo and Pozrikidis (2006) have extended the linear calculation to a wall with three-dimensional corrugations. More abrupt wall topography changes have also been considered in the limit of creeping flow, both by lubrication theory and direct numerics (Kalliadasis et al., 2000; Mazouchi and Homsy, 2001; Gaskell et al., 2004; Davis and Troian, 2005).

Bontozoglou and co-workers have studied extensively the interaction of viscous film flow down periodic corrugations with capillary-gravity waves. For small amplitudes of the bottom corrugation (linear wall) and rather thick films they found numerically a resonance (or, possibly, near resonance) of the free surface with the bottom contour (Bontozoglou and Papapolymerou, 1997). The enhancement of the bottom amplitude at the free surface was rather weak, with maximum relative amplitude that does not exceed a factor three. Later, Bontozoglou (2000) studied numerically the effect of the steepness of the bottom contour and calculated a skewed, bistable resonance with increasing steepness. This flow regime is related to the classical inviscid problem of the resonance in a liquid current over an undulated bed (Miles, 1986; Kirby, 1988; Sammarco et al., 1994).

In an experimental study of film flow over rectangular corrugations, Vlachogiannis and Bontozoglou (2002) found evidence of resonance with the bottom contour. Higher harmonics in the free surface could be traced back to those of the bottom. While Bontozoglou and co-workers focused on resonance in rather thick films in the capillary and capillary-gravity regime, Wierschem and Aksel (2004a) studied experimentally the resonance in relatively thin films in the gravity-wave regime. In this case the film thickness was about the same as the amplitude of the bottom undulation.

Despite the above experimental and numerical progress, there is yet no understanding of the mechanisms responsible for linear resonance and no systematic parametric study of the phenomenon. Such an understanding is also essential as a proper framework for investigating the nonlinear flow modifications caused by large wall deformations. Steady solutions along corrugated walls are important even when unstable, because the instability is typically convective and thus the basic flow structure is expected to persist.

In the present article, we combine numerical and analytical approaches towards a complete delineation of the steady flow behaviour over a two-dimensional weakly corrugated wall. In Section 2, we derive the governing equation, which is a variant of Orr–Sommerfeld equation with inhomogeneous boundary conditions. We solve it numerically in Section 3, performing an extensive study of the effect of the relevant dimensionless numbers. Qualitatively different branches are identified, corresponding respectively to films with small, intermediate and large thickness as compared to the corrugation length. In Section 4, we

approximate the Orr–Sommerfeld equation and solve the approximate version analytically. In the limit case of high Reynolds numbers, we recover the different branches and identify the respective physical mechanisms. Computational and analytic results converge to the same physical explanation of the resonance, which is discussed in Section 5 in the frame of the different branches identified. Finally, the conclusions are summarized in Section 6.

2. Governing equations for linear resonance

We study the two-dimensional film flow of an incompressible and Newtonian liquid down a sinusoidal bottom $b(x) = a \cos(2\pi x/\lambda)$, with wavelength λ and amplitude a . Axis x is the Cartesian coordinate in main flow direction, which is inclined at an angle α with respect to the horizontal, as shown in Fig. 1.

Denoting the position of the free surface, the bottom contour, time, pressure, and the velocity components parallel and perpendicular to the mean flow direction by $f, b, t, p, u,$ and $w,$ respectively, we apply the following ‘natural’ scaling:

$$\begin{aligned} x &= \frac{\lambda}{2\pi} X, & z &= hZ, & t &= \frac{1}{\langle u \rangle} \frac{\lambda}{2\pi} T \\ f &= hF, & b &= aB, & p &= \rho \langle u \rangle^2 P \\ u &= \langle u \rangle U, & w &= \frac{2\pi h}{\lambda} \langle u \rangle W \end{aligned} \quad (1)$$

where $\rho, h,$ and $\langle u \rangle$ are the liquid density, and the film thickness and mean velocity for a flow of same flow rate down a flat incline, respectively. The dimensionless quantities are denoted by capital letters. For a steady film flow down a flat incline, the film thickness and the mean flow velocity are according to the Nusselt solution

$$h = \sqrt[3]{\frac{3v\dot{q}}{g \sin \alpha}}; \quad \langle u \rangle = \frac{\dot{q}}{h} = \frac{gh^2 \sin \alpha}{3v} \quad (2)$$

where $\dot{q}, g,$ and v are the flow rate, acceleration of gravity, and the kinematic viscosity, respectively.

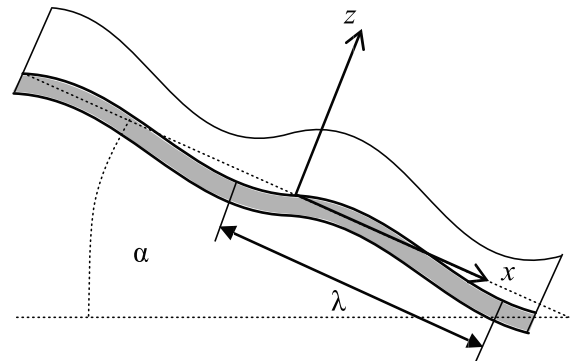


Fig. 1. Film flowing down an undulated bottom profile with wavelength λ and mean inclination angle α . The Cartesian coordinates x and z point in mean flow direction and perpendicular to it.

Applying this scaling, the Navier–Stokes equations read in dimensionless form

$$\delta Re \left(\frac{\partial U}{\partial T} + U \frac{\partial U}{\partial X} + W \frac{\partial U}{\partial Z} \right) = -\delta Re \frac{\partial P}{\partial X} + 3 + \frac{\partial^2 U}{\partial Z^2} + \delta^2 \frac{\partial^2 U}{\partial X^2} \tag{3}$$

$$\delta^2 Re \left(\frac{\partial W}{\partial T} + U \frac{\partial W}{\partial X} + W \frac{\partial W}{\partial Z} \right) = -Re \frac{\partial P}{\partial Z} - 3 \cot \alpha + \delta^3 \frac{\partial^2 W}{\partial X^2} + \delta \frac{\partial^2 W}{\partial Z^2} \tag{4}$$

where we introduced the Reynolds number for a flat incline $Re = \langle u \rangle h / \nu$, and the dimensionless film thickness $\delta = 2\pi h / \lambda$. The latter may equivalently be interpreted as a dimensionless wavenumber. The continuity equation takes the form,

$$\frac{\partial U}{\partial X} + \frac{\partial W}{\partial Z} = 0 \tag{5}$$

In integral form mass conservation yields the dimensionless flow rate

$$\dot{Q} = \int_{\xi B}^F U dZ = 1 \tag{6}$$

The field equations are complemented with the boundary conditions, which are the no-slip and no-penetration condition at the bottom

$$U = W = 0 \tag{7}$$

the kinematic boundary condition at the free surface

$$\frac{\partial F}{\partial T} + U \frac{\partial F}{\partial X} - W = 0 \tag{8}$$

and the dynamic boundary condition at the free surface. Neglecting the viscosity of air, the dynamic boundary condition reads

$$\left[Re(P - P_{\text{Air}}) + 3Bo^{-1} \frac{\frac{\partial^2 F}{\partial X^2}}{\left[1 + \left(\delta \frac{\partial F}{\partial X}\right)^2\right]^{\frac{3}{2}}} - \left(2\delta \frac{\partial U}{\partial X} \quad \delta^2 \frac{\partial W}{\partial X} + \frac{\partial U}{\partial Z} \right) \right] \vec{n} = 0 \tag{9}$$

where P_{Air} is the atmospheric pressure and where we introduced the inverse Bond number $Bo^{-1} = (2\pi l_{\text{Ca}})^2 / (\lambda^2 \sin \alpha)$ with capillary length $l_{\text{Ca}} = \sqrt{\sigma / (\rho g)}$ and surface tension σ . With the unity vectors in normal and tangential direction to the surface

$$\vec{n} = \frac{\vec{e}_Z - \delta \frac{\partial F}{\partial X} \vec{e}_X}{\sqrt{1 + \left(\delta \frac{\partial F}{\partial X}\right)^2}}, \quad \vec{t} = \frac{\vec{e}_X + \delta \frac{\partial F}{\partial X} \vec{e}_Z}{\sqrt{1 + \left(\delta \frac{\partial F}{\partial X}\right)^2}} \tag{10}$$

respectively, the projection tangential to the surface reads

$$\left[1 - \left(\delta \frac{\partial F}{\partial X} \right)^2 \right] \left(\delta^2 \frac{\partial W}{\partial X} + \frac{\partial U}{\partial Z} \right) + 4\delta^2 \frac{\partial F}{\partial X} \frac{\partial W}{\partial Z} = 0 \tag{11}$$

where we made use of the continuity equation (5). In direction normal to the surface, the projection of the dynamic boundary condition reads

$$\begin{aligned} Re(P - P_{\text{Air}}) + 3Bo^{-1} \frac{\frac{\partial^2 F}{\partial X^2}}{\left[1 + \delta^2 \left(\frac{\partial F}{\partial X}\right)^2\right]^{\frac{3}{2}}} \\ = 2\delta \frac{\partial W}{\partial Z} - \delta \frac{\partial F}{\partial X} \left(\delta^2 \frac{\partial W}{\partial X} + \frac{\partial U}{\partial Z} \right) \end{aligned} \tag{12}$$

where we made use of (5) and (11).

Considering steady flow and bottom contours with corrugation amplitudes much smaller than the film thickness ($\xi := a/h \ll 1$), we expand all quantities in a power series in ξ ,

$$\begin{aligned} U &= U_0 + \xi U_1 + O(\xi^2) \\ W &= W_0 + \xi W_1 + O(\xi^2) \\ P &= P_0 + \xi P_1 + O(\xi^2) \\ F &= F_0 + \xi F_1 + O(\xi^2) \end{aligned} \tag{13}$$

After approximating the boundary conditions by a Taylor series around the flat bottom and the leading-order solution for the position of the free surface, we arrive at leading order in ξ at the Nusselt solution for a steady film flow down a flat incline with the dimensionless velocity $U_0(Z) = 3(Z - Z^2/2)$. We remark that in our linear expansion the amplitude of the bottom corrugation is by definition much smaller than both the wavelength and the film thickness. This allows examining also thick films, where δ is of order 1, without exceeding the limit of analytic continuation of the Taylor expansion.

We replace the first-order velocity components U_1 and W_1 by introducing the dimensionless stream function $\Psi_1(X, Z)$. For the steady flow over a periodic bottom, a natural assumption is that the stream function has the same periodicity as the bottom. Thus, we express the stream function as $\Psi_1(X, Z) = \phi(Z)e^{iX}$. After cross-differentiating the X and Z components of the Navier–Stokes equation to eliminate pressure, we derive the Orr–Sommerfeld equation for zero phase velocity,

$$\phi_{zzzz} - 2\delta^2 \phi_{zz} + \delta^4 \phi = i\delta Re [U_0(\phi_{zz} - \delta^2 \phi) - U_{0zz} \phi] \tag{14}$$

where the subscript Z denotes differentiation with respect to the Cartesian coordinate Z .

Next, we describe the response of the free surface at first-order in ξ by the ansatz

$$F_1 = Ae^{iX} \tag{15}$$

where A is the relative amplitude of the free surface to that of the wall. The ansatz (15) is related to the assumptions of small wall amplitude and of steady film flow. Thus, when the Reynolds number is high enough for the flow to become unstable, the steady solutions presently considered are not realizable in a strict sense. However, we must note that such solutions are still important because film instabilities are typically convective. As a consequence, disturbances affect the flow only temporarily as they move

downstream, and the steady flow re-establishes. This point is further elaborated in Section 5.

Applying (13) and (15), the boundary conditions (7), (8), (11) and (12) read

$$\phi(0) = 0 \tag{16}$$

$$\phi_z(0) = -3 \tag{17}$$

$$\phi(1) = -\frac{3}{2}A \tag{18}$$

$$\phi_{zz}(1) + (2 + \delta^2)\phi(1) = 0 \tag{19}$$

$$i\phi_{zzz}(1) + \left(\frac{3}{2}\delta Re - i3\delta^2\right)\phi_z(1) = 2\delta(\cot\alpha + Bo^{-1})\phi(1) \tag{20}$$

where we replaced A in (19) and (20) using the kinematic boundary condition (18) and eliminated the pressure from the dynamic boundary condition by differentiating it with respect to X and inserting the X -component of the Navier–Stokes equation.

The set of Eqs. (14)–(20) contains four dimensionless parameters: Re , δ , $\cot\alpha$, and Bo^{-1} . Eq. (20) shows that in the linear limit considered here $\cot\alpha$ and Bo^{-1} , which describe the effects of the hydrostatic and the capillary pressures, sum up to a single parameter, the pressure number $P_{hc} = \cot\alpha + Bo^{-1}$, reducing the independent parameters to three. Thus, in what follows we consider the two pressure terms as a single parameter without analysing the effects independently. We note that Reynolds number and pressure terms only enter as products with the film-thickness parameter δ leading to reduced inertia and pressure terms. As is apparent from (14), viscous friction is mainly due to wall shear in thin films, where $\delta^2 \ll 1$, and the convective term that transports changes in the vertical velocity component is negligible. The latter as well as viscous damping gains importance in thicker films.

With respect to the connection between the present parametric analysis and possible experimental realization of the flow, we find it more convenient to think in terms of a specific wall with fixed wavelength. This also fixes the inverse Bond number and makes the interpretation of δ as a dimensionless film thickness more appealing than that of a dimensionless wavenumber. The two remaining

parameters, Re and δ , may be varied independently only by controlling both the flow rate and the viscosity of the liquid.

To the best of our knowledge it is not possible to obtain for the Orr–Sommerfeld equation (14) an analytic solution in closed form. This is due to the dependence of the velocity U_0 on the Z coordinate. Numerically, the system (14)–(20) can be solved in a straightforward way. We use a centred finite-difference scheme with equidistant discretisation.

3. Numerical results

Fig. 2 shows the free-surface amplitude relative to that of the wall as a function of the Reynolds number for different magnitudes of the pressure number and the dimensionless film thickness. As is typical for resonance, all curves show a local maximum for the amplitude at a certain Reynolds number, which we call the resonant Reynolds number Re_{res} . According to Fig. 2a, the resonance is stronger at film thickness of about one. For thinner films the maximum flattens progressively, whereas for thicker films the maximum retains its sharpness but diminishes in amplitude. According to Fig. 2b, the free-surface amplitude increases with the pressure number, and the region of strong response moves to higher Reynolds numbers.

The dependence of the resonance on the film thickness is more subtle than can be appreciated by the few results above. Generally, the resonance sharpens with increasing film thickness. But depending on the magnitudes of the pressure terms and on the film-thickness range, the amplitude and the Reynolds number at resonance may decrease or increase with increasing film thickness. Thus, Fig. 3 is a detailed parametric study that illustrates how amplitude and resonant Reynolds number depend on the film thickness for different magnitudes of the pressure number.

Fig. 3a shows the maximum amplitude of the free surface and indicates that three different regimes are apparent: (i) For thin films the maximum amplitude increases with the film thickness and also with the pressure number. In

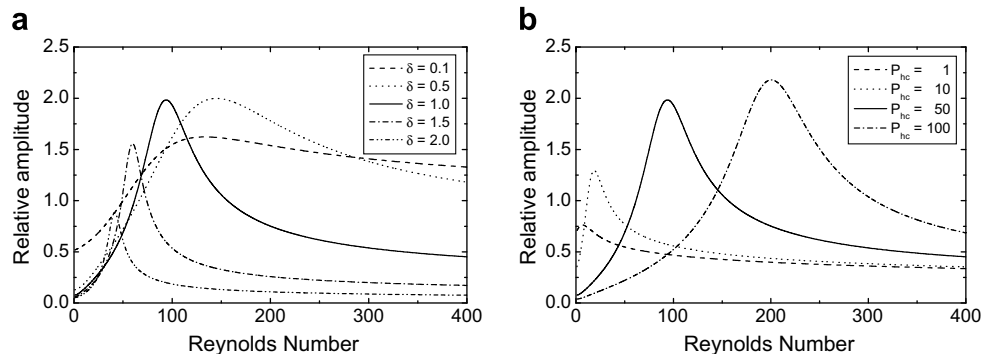


Fig. 2. Resonance curves for different film thicknesses at pressure number $P_{hc} = 50$ (a), and for different pressure numbers at film thickness $\delta = 1$ (b).

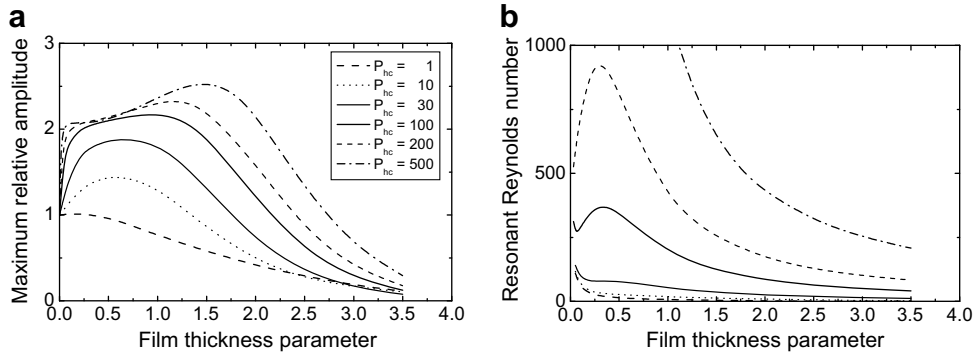


Fig. 3. Maximum free-surface amplitude, i.e. free-surface amplitude at $Re = Re_{res}$, as a function of the film-thickness parameter δ for different pressure numbers (a) and the resonant Reynolds number (b) from the numerical solution of the set of Eqs. (14)–(20).

the limit of very thin films the free surface follows closely the wall and thus its relative amplitude approaches everywhere the value one. This behaviour occurs as long as there are no recirculation zones in the corrugation troughs, a condition valid by definition in the present study of a linearly deformed wall. (ii) For thick films, resonance diminishes with film thickness and eventually tends to zero. In this regime the effect of pressure number is only roughly monotonic, exhibiting a minimum at a small but nonzero value of the pressure number. (iii) The intermediate region of order one film thickness appears, at low pressure numbers, to balance the above counteracting trends of thin and thick films and to lead to a smooth maximum. However, for $P_{hc} \sim O(10^2)$, the intermediate region exhibits distinct saturation resulting in a plateau of the maximum amplitude insensitive to further increase in the pressure number. We consider this saturated region as the third branch of the solution.

Fig. 3b shows the Reynolds number at resonance. For pressure numbers of the order of 10^1 , the Reynolds number at resonance is of the order of 10^2 and decreases with the film thickness. For pressure numbers of about 10^2 , however, this decline in the Reynolds number for the maximum free surface amplitude is only found for the thinnest films. After a sharp local minimum the Reynolds number increases again up to a local maximum and only diminishes for thick films. For higher pressure numbers the decline for

thin films is limited to very small thicknesses, not resolvable in the figure.

4. Analytical approximation for the Orr–Sommerfeld equation

Since it is not possible to obtain an exact analytic solution for the Orr–Sommerfeld equation (14) due to the dependence of the velocity U_0 on the Z coordinate, we now search for an approximate analytical solution. To obtain approximate solutions for the Orr–Sommerfeld equation, Anshus and Goren (1966) proposed to replace this velocity by the velocity at the free surface while keeping the second derivative of U_0 at its true value. In this section we apply this approach to the linear resonance described by the set of Eqs. (14)–(20) and consider the limit case of high Reynolds numbers.

Replacing $U_0(Z)$ in the Orr–Sommerfeld equation (14) by the surface velocity of the Nusselt solution, $3/2$, the approximated Orr–Sommerfeld equation

$$\phi_{zzzz} - 2\delta^2\phi_{zz} + \delta^4\phi = \frac{3}{2}i\delta Re[\phi_{zz} + (2 - \delta^2)\phi] \quad (21)$$

is solved by

$$\phi = c_{11} \exp(\beta_1 Z) + c_{12} \exp(-\beta_1 Z) + c_{21} \exp(\beta_2 Z) + c_{22} \exp(-\beta_2 Z) \quad (22)$$

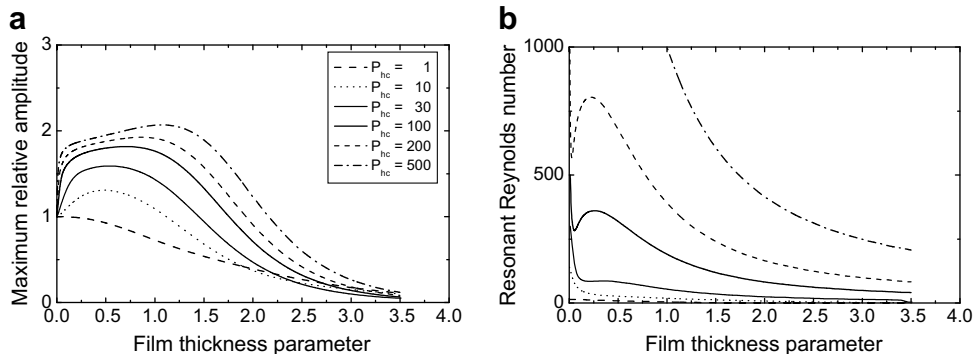


Fig. 4. Maximum amplitude of the free surface (a) and the resonant Reynolds number (b) from the approximate Orr–Sommerfeld equation (21).

with

$$\beta_1 = \sqrt{i\frac{3}{4}\delta Re + \delta^2 - \sqrt{\left(i\frac{3}{4}\delta Re\right)^2 + 4\left(i\frac{3}{4}\delta Re\right)}} \quad (23)$$

$$\beta_2 = \sqrt{i\frac{3}{4}\delta Re + \delta^2 + \sqrt{\left(i\frac{3}{4}\delta Re\right)^2 + 4\left(i\frac{3}{4}\delta Re\right)}}$$

The constants c_{ij} in (22) are determined from the boundary conditions (16)–(20) and finally the complex relative amplitude A is obtained. The procedure is conceptually straight forward but laborious. Thus, it is done with the help of computer algebra software (Maple 11.0) and the final result for the relative amplitude is given in Appendix A. Fig. 4 shows the maximum relative amplitude and the resonant Reynolds number predicted by this analytic solution of the approximate Orr–Sommerfeld equation (21). Apparently, the solution retains all qualitative features of the exact linear resonance. In particular, the three branches for thin films, for intermediate films at high pressure numbers, and for thick films are contained by the analysis.

The different regimes for the resonance have been classified on the basis of the film-thickness parameter δ . In the set of Eqs. (16)–(21), the parameter enters in three ways: (i) It rescales the Reynolds number and the pressure number, (ii) it scales viscous damping in (19)–(21), and (iii) it governs the importance of the convective term $-(3/2)i\delta Re\delta^2\phi$ in (21).

Next, we try to understand the above behaviour by an asymptotic expansion of the analytic solution (22), in the limit of high Reynolds numbers. The validity of such an expansion is justified by Fig. 4b, which shows that the resonant Reynolds number is quite high for large pressure numbers. We start with the general expression for the relative amplitude, A , given in (A.1) of Appendix A, and retain the leading-order term in $\sqrt{\delta Re}$ in the numerator and the first three orders in $\sqrt{\delta Re}$ in the denominator. As will be seen next, these three orders are sufficient to capture the main characteristics of the resonance. Assuming that P_{hc} and Re are of comparable magnitude yields

Details of the derivation are given in Appendix B. Grouping terms according to the order of approximation, we write (24) as

$$A = \frac{3\delta Re\sqrt{\delta^2 - 2}}{(\delta Re)^{3/2}a_1 + (\delta Re)a_2 + (\delta Re)^{1/2}a_3} \quad (25)$$

where a_1, a_2, a_3 are functions of δ and the ratio P_{hc}/Re .

Perfect resonance is predicted from (25) by retaining in the denominator only the leading-order term. Indeed, the following resonance condition is found at first-order by setting $a_1 = 0$:

$$Re_{res} = \frac{4}{3} \frac{P_{hc}}{\sqrt{\delta^2 - 2}} \times \frac{\exp(\sqrt{\delta^2 - 2}) - \exp(-\sqrt{\delta^2 - 2})}{\exp(\sqrt{\delta^2 - 2}) + \exp(-\sqrt{\delta^2 - 2})} \quad (26)$$

which evidently results in an infinite amplitude. According to (26), Re_{res} is proportional to δ^{-1} for very thick films and grows continuously with decreasing film thickness up to the limit $Re_{res} \approx 6P_{hc}$ for $\delta \rightarrow 0$. This relation describes accurately the observed variation of the resonant Reynolds number with film thickness (Fig. 3b and Fig. 4b) for thick films. As an example, we compare in Fig. 5b exact and asymptotic results, and confirm that the next-order term is necessary only to capture the decline in Re_{res} observed for thin films.

The above leading-order behaviour is reminiscent of the classical inviscid problem of a liquid current moving with uniform base velocity along a wavy wall (Miles, 1986; Kirby, 1988; Sammarco et al., 1994). That problem has been studied as a useful model of the dynamics of erodible beds in open channel flows (Reynolds, 1965; Mei, 1969). It is recalled that, in the inviscid limit, the no-slip boundary condition on the wall is dropped, and the resulting slip velocity is of the order of the base current. Thus, the wavy wall imparts large momentum perturbations normal to the mean flow direction, which trigger a strong resonance. The

$$A = \frac{-3\delta Re\sqrt{\delta^2 - 2}}{\left\{ \begin{aligned} &\sqrt{\frac{3}{4}\delta Re}(1+i) \left(\frac{\delta P_{hc}(\exp(\sqrt{\delta^2 - 2}) - \exp(-\sqrt{\delta^2 - 2}))}{-\frac{3}{4}\delta Re\sqrt{\delta^2 - 2}(\exp(\sqrt{\delta^2 - 2}) + \exp(-\sqrt{\delta^2 - 2}))} \right) \\ &- \sqrt{\delta^2 - 2} \left(\frac{\delta P_{hc}(\exp(\sqrt{\delta^2 - 2}) + \exp(-\sqrt{\delta^2 - 2}))}{-\frac{3}{4}\delta Re\sqrt{\delta^2 - 2}(\exp(\sqrt{\delta^2 - 2}) - \exp(-\sqrt{\delta^2 - 2}))} \right) \\ &+ \sqrt{\frac{3}{4}\delta Re}(1-i) \left(\frac{\delta P_{hc}\left(\frac{10+\delta^2}{3\delta Re}\right)(\exp(\sqrt{\delta^2 - 2}) - \exp(-\sqrt{\delta^2 - 2}))}{-\frac{3}{4}\delta Re\sqrt{\delta^2 - 2}\left(\frac{1}{3\delta Re} - \frac{24-4\delta^2+9\delta^4}{\delta^2-2}\right)(\exp(\sqrt{\delta^2 - 2}) + \exp(-\sqrt{\delta^2 - 2}))} \right) \end{aligned} \right\}} \quad (24)$$

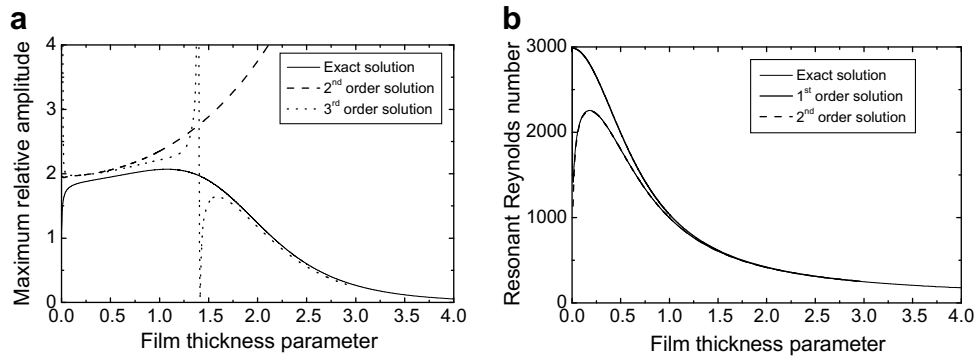


Fig. 5. Comparison of the maximum amplitude of the free surface (a) and the resonant Reynolds number (b) between the analytical solutions of the approximate Orr–Sommerfeld equation (21) and the limiting cases of (24) at high Reynolds number for different orders of approximation. $P_{hc} = 500$.

parallelism is further strengthened by noting that an inviscid approximation of the present formulation (i.e. neglecting the viscous terms in (20) and (21), and dropping (17) and (19) leads precisely to the resonance condition (26).

Returning to Eq. (24), we note that the second- and third-order terms detune the perfect resonance, and thus reduce the influence of the wall deformation on the free surface. The changes, with increasing order of approximation, in the predicted relative amplitude and resonant Reynolds number are demonstrated in Fig. 5 for the representative case $P_{hc} = 500$. Fig. 5a shows that, with the addition of the second-order term, the relative amplitude for films of intermediate thickness (i.e. the saturation region) is correctly predicted. However, there is growing deviation for thick films. Fig. 5b shows that the addition of the second-order term reveals the local maximum in the resonant Reynolds number and the subsequent decline with decreasing film thickness. Finally, from Fig. 5a, we note that inclusion of the third-order term in the high-Re expansion (24) also captures the decline of the relative amplitude in thick films. Thus, the first three orders in $\sqrt{\delta Re}$ in the denominator of (24) suffice to describe the main resonance characteristics.

There are two regions, however, that are not properly accounted for: (i) In the limit of very thin films ($\delta < 0.1$), there occurs, with decreasing film thickness, an abrupt decline of the relative amplitude towards the value one and an equally abrupt rise in the resonant Reynolds number. Though Fig. 4 confirms that this trend is present in the full analytic solution (22), it is not recovered up to the third-order. (ii) The asymptotics are derived with the assumption that term $\sqrt{\delta^2 - 2}$ is of order one, thus a singularity appears at third-order at $\delta = \sqrt{2}$ (Fig. 5a). As this singularity affects only a narrow range of film thicknesses, inclusion of even higher terms in order to remove it does not appear justifiable.

It is evident from the above discussion and also from looking at Eq. (24), that a change of behaviour takes place by crossing the dimensionless film thickness $\delta = \sqrt{2}$. This change can be traced back to the change in sign of the ϕ -terms on the right-hand side of the Orr–Sommerfeld

equation (21) and thus to the convective coupling between the leading-order flow velocity U_0 and the velocity perturbation perpendicular to the mean flow direction W_1 , which transports the perturbation caused by the bottom undulation to the free surface. For $\delta < \sqrt{2}$, the coupling is efficient but the rescaling by δ of the Reynolds and pressure numbers makes the resonance broader and weaker. For $\delta > \sqrt{2}$, the efficiency of transportation of the bottom perturbation towards the free surface gradually deteriorates. As a result, the resonance remains sharp but declines in amplitude.

5. Discussion

The steady flow of a liquid film along a wavy wall is described, in the limit of small amplitude corrugations, by an Orr–Sommerfeld equation with zero phase velocity (14). This coincidence points to a connection between the presently investigated linear resonance and the stability analysis of film flow along a flat wall. Similar to the situation of vibrating walls (Floryan et al., 2002), the weakly wavy wall may be viewed as a forcing function for Nusselt flow, which will produce significant effects only if it happens to be in synchrony with one of its eigenmodes. In this respect, we are interested in a mode with the same wavelength as the wall and with zero phase velocity. Such a mode could potentially extract energy from the spatially steady modulations imposed on the base flow by the wavy wall.

To study this point further, we consider the full Orr–Sommerfeld equation

$$\phi_{zzzz} - 2\delta^2\phi_{zz} + \delta^4\phi = i\delta Re[(U_0 - C)(\phi_{zz} - \delta^2\phi) - U_{0zz}\phi] \quad (27)$$

where C is the dimensionless phase velocity of the disturbance, and solve it with a standard numerical technique subject to the appropriate *homogenous* boundary conditions at the wall and the free surface. As a representative example, we take $P_{hc} = 50$ and $\delta = 1.0$, i.e. we consider the temporal stability of a flat film subjected to a disturbance of wavelength corresponding to the above value of

δ . Fig. 6 shows the real and imaginary part of the phase velocity of the least stable modes for $Re = 50$, $Re = 92.6$ and $Re = 135.2$.

There are always two surface modes in Fig. 6, which correspond to capillary-gravity waves travelling in the positive and negative direction with respect to the mean flow. The fast wave is the well-known source of interfacial instability, which leads to the kinematic surface waves not accounted for in the steady flow considered in this paper. The slow wave is always weakly damped, but its phase velocity is observed to shift from negative to positive values. Most notably, it is exactly zero at the Reynolds number that leads to maximum steady response in film flow along a wavy wall with $P_{hc} = 50$ and $\delta = 1$ (see Fig. 2). This coincidence supports the conclusion that resonance is caused by energy transfer to the capillary-gravity wave that is travelling against the mean flow and thus may remain steady in the laboratory frame of reference.

We note that the resonant deformation of the free surface is important even under conditions that lead to

growth of the fast travelling eigenmode, i.e. when the steady film flow is unstable. This happens because the instability is convective, and the steady deformation forms the base flow on which the kinematic waves travel. Indeed, it has been experimentally confirmed by Argyriadi et al. (2006) that the resonant deformation is a dominant feature of the free surface, and is only slightly modulated in amplitude and phase during the passage of travelling waves.

The above relation between steady resonance and capillary-gravity modes helps understand the change in resonance sharpness with dimensionless film thickness. Waves are almost non-dispersive on very thin films, i.e. their phase velocity varies weakly with the parametric conditions. As a result, the resonance is broad. On the contrary, the strongly dispersive nature of waves on thicker films assures that only a narrow range around perfect tuning ($C = 0$) is significantly amplified.

6. Conclusions

We study steady flow of a liquid film along a corrugated wall in the linear limit of infinitesimal corrugation amplitude. This flow is parameterized by the Reynolds number, the pressure number (sum of hydrostatic and capillary contributions) and the dimensionless film thickness, and is described by an Orr–Sommerfeld equation with zero phase velocity and inhomogeneous boundary conditions.

A numerical investigation shows that the resonance is rather weak (with free surface amplitude not exceeding three times that of the wall), and that it is broad in thin films and sharp in thick films. In thin films the amplitude increases with the film thickness, whereas it decreases in thick films. The resonance generally strengthens with the pressure number, P_{hc} , but when $P_{hc} \sim O(10^2)$ a saturation plateau develops at intermediate film thicknesses where the amplitude does not change with further increase in P_{hc} .

Approximating the leading-order (semi-parabolic) velocity profile in the Orr–Sommerfeld equation by the free surface value allows for an analytic solution, which retains the qualitative features of the exact linear results. An asymptotic expansion of the analytic solution in the limit of high Reynolds numbers, reveals the relevant physical mechanisms: at first-order, the classical inviscid resonance of a uniform current is recovered, which predicts correctly the resonant Reynolds number for thick and intermediate films but has infinite relative amplitude (perfect tuning). Second and third-order terms detune perfect resonance and account for almost all the main characteristics. The second-order correction is related to the rescaling by δ of the Reynolds and pressure numbers, and is significant for thin films. The third-order correction is related to the convective coupling of the leading-order velocity to the component perpendicular to the mean flow direction. Thus, it accounts for the gradual deterioration in the efficiency of

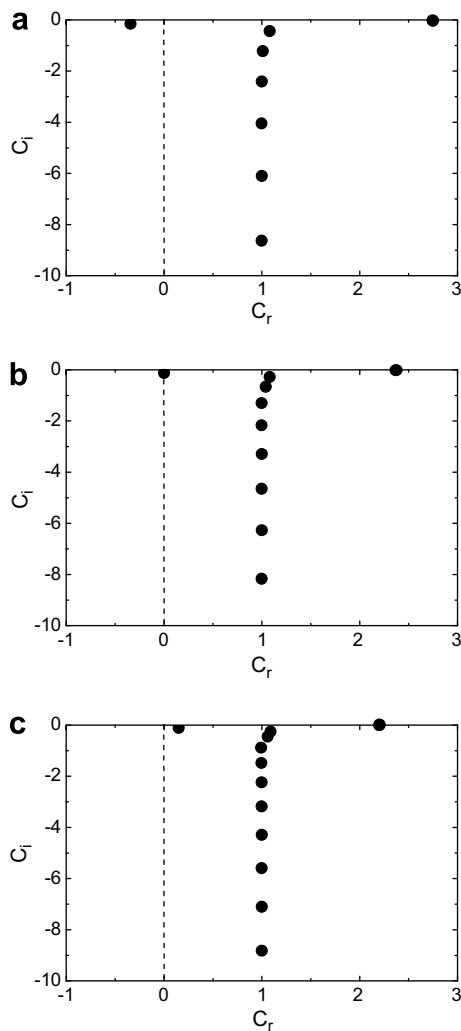


Fig. 6. The real and imaginary parts of the phase velocity of the least stable linear eigenmodes for film flow along a flat wall at $P_{hc} = 50$ and $\delta = 1$. Results for $Re = 50$ (a), $Re = 92.6$ (b), and $Re = 135.2$ (c).

the flow to transport wall perturbations towards the free surface.

Our results support the view that the resonance is associated with the interaction of the undulated film with capillary-gravity waves travelling against the mean flow direction. As a consequence, the resonance peak is attained under conditions that render the wave phase velocity equal to zero in the laboratory reference frame, and thus permit direct exchange of energy between the steadily deformed film and the free surface.

Appendix A. Analytic solution of the approximate Orr–Sommerfeld equation

Complex relative amplitude:

$$A = \frac{6(\beta_2^2 - \beta_1^2)[n_2(\exp(\beta_1) - \exp(-\beta_1)) - n_1(\exp(\beta_2) - \exp(-\beta_2))]}{\left\{ \begin{aligned} &\delta P_{hc}[G_1(\exp(\beta_1 + \beta_2) - \exp(-\beta_1 - \beta_2)) + G_2(\exp(\beta_1 - \beta_2) - \exp(-\beta_1 + \beta_2))] \\ &+ \frac{3}{2}[G_3(\exp(\beta_1 + \beta_2) + \exp(-\beta_1 - \beta_2)) + G_4(\exp(\beta_1 - \beta_2) + \exp(-\beta_1 + \beta_2))] + 3G_5 \end{aligned} \right\}} \tag{A.1}$$

where

$$\begin{aligned} G_1 &:= \beta_1^3 + \beta_2^3 - \beta_1\beta_2(\beta_1 + \beta_2) \\ G_2 &:= -(\beta_1^3 - \beta_2^3) - \beta_1\beta_2(\beta_1 - \beta_2) \\ G_3 &:= -(\beta_1 - \beta_2)(n_2t_1 - n_1t_2) \\ G_4 &:= -(\beta_1 + \beta_2)(n_2t_1 + n_1t_2) \\ G_5 &:= \beta_1n_2t_2 + \beta_2n_1t_1 \\ n_1 &:= \beta_1 \left(\frac{1}{2} \delta Re + i \frac{1}{3} \beta_1^2 - i \delta^2 \right) \\ n_2 &:= \beta_2 \left(\frac{1}{2} \delta Re + i \frac{1}{3} \beta_2^2 - i \delta^2 \right) \\ t_1 &:= \beta_1^2 + \delta^2 + 2 \\ t_2 &:= \beta_2^2 + \delta^2 + 2 \end{aligned} \tag{A.2}$$

with β_1 and β_2 given by (23).

Appendix B. Limit case approximations for high Reynolds numbers

Expanding β_1 and β_2 for large Reynolds numbers and with δ being of order one, we arrive from (23) at

$$\begin{aligned} \beta_1 &= \sqrt{\delta^2 - 2 + \frac{2}{i\frac{3}{4}\delta Re} + O\left(\frac{1}{(\delta Re)^2}\right)} \\ \beta_2 &= \sqrt{2i\frac{3}{4}\delta Re + \delta^2 + 2 - \frac{2}{i\frac{3}{4}\delta Re} + O\left(\frac{1}{(\delta Re)^2}\right)} \end{aligned} \tag{B.1}$$

i.e. $\beta_2 = O(\sqrt{\delta Re})$ and β_1 is of order one unless $\delta \approx \sqrt{2}$, where $\beta_1 = O((\delta Re)^{-1/2})$. In the following

considerations of the limit case study we assume β_1 to be of order one, i.e. excluding the case $\delta \approx \sqrt{2}$. Thus, retaining for the relative amplitude from (A.1) only terms with $\exp(\beta_2)$ and neglecting the rest we arrive at

$$A = \frac{-6(\beta_2^2 - \beta_1^2)n_1}{\delta P_{hc}[G_1 \exp(\beta_1) - G_2 \exp(-\beta_1)] + \frac{3}{2}[G_3 \exp(\beta_1) + G_4 \exp(-\beta_1)]} \tag{B.2}$$

where $\exp(\beta_2)$ has cancelled out. Inserting G_1 – G_4 according to (A.2) and arranging the terms in the numerator and the denominator in powers of the square root of the Reynolds number, the complex amplitude reads now

$$A = \frac{3\delta Re\beta_2^2\beta_1 + i6\beta_2^2\beta_1(\frac{1}{3}\beta_1^2 - \delta^2) - 3\delta Re\beta_1^3 - i6\beta_1^3(\frac{1}{3}\beta_1^2 - \delta^2)}{\left\{ \begin{aligned} &-\delta P_{hc} \left[\begin{aligned} &\beta_2^3(\exp(\beta_1) - \exp(-\beta_1)) - \beta_2^2\beta_1(\exp(\beta_1) + \exp(-\beta_1)) \\ &-\beta_2\beta_1^2(\exp(\beta_1) - \exp(-\beta_1)) + \beta_1^3(\exp(\beta_1) + \exp(-\beta_1)) \end{aligned} \right] \\ &+ \frac{3}{2} \left[\begin{aligned} &\beta_2 \left(\begin{aligned} &\frac{1}{2} \delta Re \beta_2^2 \beta_1 \\ &+ \frac{1}{2} \delta Re \beta_1 (\beta_1^2 + 2\delta^2 + 4) + i\frac{2}{3} \beta_2^2 \beta_1 (\beta_1^2 - \delta^2 + 1) \\ &+ i\beta_1 \left((\frac{1}{3} \beta_1^2 - \delta^2) (\delta^2 + 2) - \delta^2 (\beta_1^2 + \delta^2 + 2) \right) \end{aligned} \right) (\exp(\beta_1) + \exp(-\beta_1)) \\ &- \left(\begin{aligned} &\beta_2^2 (\frac{1}{2} \delta Re (2\beta_1^2 + \delta^2 + 2) + i\frac{1}{3} \beta_2^2 (\beta_1^2 + \delta^2 + 2)) \\ &+ \frac{1}{2} \delta Re \beta_1^2 (\delta^2 + 2) + i\beta_2^2 (\beta_1^2 (\frac{1}{3} \beta_1^2 - \delta^2) - \delta^2 (\beta_1^2 + \delta^2 + 2)) \end{aligned} \right) (\exp(\beta_1) - \exp(-\beta_1)) \\ &+ i\beta_1^2 (\frac{1}{3} \beta_1^2 - \delta^2) (\delta^2 + 2) \end{aligned} \right] \end{aligned} \right\}} \tag{B.3}$$

where β_2 -terms were arranged according to their leading order in the Reynolds number. The dependence on β_2 shows that numerator and denominator are power series in $\sqrt{\delta Re}$.

Since resonance is mainly governed by the denominator, we retain only the leading-order term for the numerator but consider the first three orders in $\sqrt{\delta Re}$ in the denominator, assuming that P_{hc} and Re are of comparable order. After inserting β_1 and β_2 from (B.1) and arranging the denominator in real and imaginary parts, we finally arrive at (24).

References

- Anshus, B.E., Goren, S.L., 1966. A method of getting approximate solutions to the Orr–Sommerfeld equation for flow on a vertical wall. *AIChE J.* 12, 1004–1009.
- Argyriadi, K., Vlachogiannis, M., Bontozoglou, V., 2006. Experimental study of inclined film flow along periodic corrugations: the effect of wall steepness. *Phys. Fluids* 18, 012102.
- Benjamin, T.B., 1957. Wave formation in laminar flow down an inclined plane. *J. Fluid Mech.* 2, 554–574.
- Bontozoglou, V., 2000. Laminar film flow along a periodic wall. *Comp. Model. Eng. Sci.* 1, 133–142.
- Bontozoglou, V., Papapolymerou, G., 1997. Laminar film flow down a wavy incline. *Int. J. Multiphas. Flow* 23, 69–79.
- Chang, H.-C., 1994. Wave evolution on a falling film. *Ann. Rev. Fluid Mech.* 26, 103–136.
- Davis, J.M., Troian, S.M., 2005. Generalized linear stability of noninertial coating flows over topographical features. *Phys. Fluids* 17, 072102.
- deSantos, J.M., Melli, T.R., Scriven, L.E., 1991. Mechanics of gas–liquid flow in packed-bed contactors. *Ann. Rev. Fluid Mech.* 23, 233–260.
- Floryan, J.M., Davis, S.H., Kelly, R.E., 1987. Instabilities of a liquid film flowing down a slightly inclined plane. *Phys. Fluids* 30, 983–989.
- Floryan, J.M., Szumbariski, J., Wu, X., 2002. Stability of flow in a channel with vibrating walls. *Phys. Fluids* 14, 3927–3936.
- Focke, W.W., Knibbe, P.G., 1986. Flow visualization in parallel-plate ducts with corrugated walls. *J. Fluid Mech.* 165, 73–77.
- Gaskell, P.H., Jimack, P.K., Sellier, M., Thompson, H.M., Wilson, M.C.T., 2004. Gravity-driven flow of continuous thin liquid films on non-porous substrates with topography. *J. Fluid Mech.* 509, 253–280.
- Kalliadasis, S., Bielarz, C., Homsy, G.M., 2000. Steady free-surface thin film flows over topography. *Phys. Fluids* 12, 1889–1898.
- Kang, F., Chen, K., 1995. Gravity-driven two-layer flow down a slightly wavy periodic incline at low Reynolds numbers. *Int. J. Multiphas. Flow* 21, 501–513.
- Kirby, J.T., 1988. Current effects on resonant reflection of surface water waves by sand bars. *J. Fluid Mech.* 186, 501–520.
- Lin, S.P., 1967. Instability of a liquid film flowing down an inclined plane. *Phys. Fluids* 10, 308–313.
- Luo, H.X., Pozrikidis, C., 2006. Effect of inertia on film flow over oblique and three-dimensional corrugations. *Phys. Fluids* 18, 078107.
- Malamataris, N.A., Bontozoglou, V., 1999. Computer aided analysis of viscous film flow along an inclined wavy wall. *J. Comput. Phys.* 154, 372–392.
- Mazouchi, A., Homsy, G.M., 2001. Free surface Stokes flow over topography. *Phys. Fluids* 13, 2751–2761.
- Mei, C.C., 1969. Steady free surface flow over a wavy bed. *J. Eng. Mech., Proc. Am. Soc. Civil Eng. EM* 6, 1393–1402.
- Miles, J.W., 1986. Weakly nonlinear Kelvin–Helmholtz waves. *J. Fluid Mech.* 172, 513–529.
- Negny, S., Meyer, M., Prevost, M., 2001. Study of laminar falling film flowing over a wavy column: Part I. Numerical investigation of the flow pattern and the coupled heat and mass transfer. *Int. J. Heat Mass Transf.* 44, 2137–2146.
- Reynolds, A.J., 1965. Waves on the erodible bed of an open channel. *J. Fluid Mech.* 22, 113–133.
- Roberts, A.J., Li, Z., 2006. An accurate and comprehensive model of thin fluid flows with inertia on curved substrates. *J. Fluid Mech.* 553, 33–73.
- Sammarco, P., Mei, C.C., Trulsen, K., 1994. Nonlinear resonance of free-surface waves in a current over a sinusoidal bottom – a numerical study. *J. Fluid Mech.* 279, 377–405.
- Scholle, M., Wierschem, A., Aksel, N., 2004. Creeping films with vortices over strongly undulated bottoms. *Acta Mech.* 168, 167–193.
- Shetty, L., Cerro, R.L., 1993. Flow of a thin film over a periodic surface. *Int. J. Multiphas. Flow* 18, 495–516.
- Vlachogiannis, M., Bontozoglou, V., 2002. Experiments on laminar film flow along a periodic wall. *J. Fluid Mech.* 457, 133–156.
- Wang, C.Y., 1984. Thin film flowing down a curved surface. *Z. Angew. Math. Phys.* 35, 533–544.
- Webb, R.L., 1994. Principles of Enhanced Heat Transfer. Wiley.
- Wierschem, A., Aksel, N., 2004a. Hydraulic jumps and standing waves in gravity-driven flows of viscous liquids in wavy open channels. *Phys. Fluids* 16, 3868–3877.
- Wierschem, A., Aksel, N., 2004b. Influence of inertia on vortices created in films creeping over strongly undulated substrates. *Phys. Fluids* 16, 4566–4574.
- Wierschem, A., Lepski, C., Aksel, N., 2005. Effect of long undulated bottoms on thin gravity-driven films. *Acta Mech.* 179, 41–66.
- Yih, C.-S., 1963. Stability of liquid flow down an inclined plane. *Phys. Fluids* 6, 321–334.
- Zhao, L., Cerro, R.I., 1992. Experimental characterization of viscous film flows over complex surfaces. *Int. J. Multiphas. Flow* 18, 495–516.